 ISSN 2522-1841 (Online)
ISSN 0005-2531 (Print)

DETERMINATION OF THE GLASS FORMATION REGION IN THE Bi_2O_3 - B_2O_3 - Nd_2O_3 TERNARY SYSTEM AND STUDY THE THERMAL AND ELECTROPHYSICAL PROPERTIES OF SOME ALLOYS ALONG THE Bi_2O_3 - $Nd_2O_3 \cdot B_2O_3$ SECTION

S. I. Bananyarli[1], L. A. Khalilova[1], Ch.A.Imamalizade[2], Sh. S. Ismailov[1]

[1] *"Institute of Chemistry" Public Legal Entity, MSE of the Azerbaijan Republic, Baku, Azerbaijan*
[2] *Azerbaijan State Oil and Industrial University, Baku, Azerbaijan*

ishr_az@yahoo.com

Received 16.04.2026
Reviewed 20.05.2026
Accepted 22.06.2026

In this article, the Bi_2O_3-B_2O_3-Nd_2O_3 ternary system was studied by differential thermal analysis and X-Ray diffraction technique, the boundaries of the glass formation region were determined, and the electrical and thermal properties of some alloys along the Bi_2O_3 - $Nd_2O_3 \cdot B_2O_3$ section were investigated. It was determined that the expansion of the glass transition region in the Bi_2O_3-B_2O_3-Nd_2O_3 ternary system is related to the presence of a glass forming compound of the $3Bi_2O_3 \cdot Nd_2O_3 \cdot 6B_2O_3$ system. It was found that in the sample with the composition $(Bi_2O_3)_{95}$ – $(Nd_2O_3 \cdot B_2O_3)_5$, at relatively low temperatures ($T \leq 420$ K), phonon scattering by point defects and acoustic phonons occurs. With increasing temperature, scattering by optical phonons increases, resulting in a sharp increase in thermal resistance. Therefore, the thermal conductivity and, accordingly, the electrical conductivity of this composition are very low. As a result of the experiments, it was found that the current-voltage characteristic of the sample containing $(Bi_2O_3)_{75}$–$(Nd_2O_3 \cdot B_2O_3)_{25}$ changes nonlinearly, and the electrical resistance is of the order of $R \approx 10^6 \div 10^8$ Ohm. The obtained results allow the use of the specified composition in practice in the manufacture of varistor-type thermistors in the temperature range of 300÷440 K.

Keywords: *thermal resistance, thermal conductivity, phonon, semiconductor, thermistor, varistor.*

https://doi.org/10.59849/0005-2531.2026.4.32

Introduction

The acquisition of environmentally friendly materials with high nonlinear optical sensitivity, mechanical strength, and chemical resistance, and the study of their physical properties, remain relevant [1-5]. Bismuth-containing oxide systems have attracted considerable attention owing to their ability to form a wide variety of functional materials with promising optical, dielectric, ferroelectric, and ionic-conducting properties [6-10]. Several compounds of the Bi_2O_3–B_2O_3 system, including $Bi_4B_2O_9$, $Bi_6B_{10}O_{24}$, BiB_3O_6, and $Bi_2B_8O_{15}$, have been identified as promising materials for optical and photonic applications [8, 9]. Among them, bismuth borates constitute an important class of compounds characterized by high refractive indices, significant nonlinear optical coefficients and relatively low synthesis temperatures [11-19].

Rare-earth borates represent another important family of functional materials owing to their excellent optical, luminescent and laser characteristics. Neodymium-containing borates are of particular interest because Nd^{3+} ions exhibit intense electronic transitions in the visible and near-infrared regions, making them attractive for solid-state laser and photonic applications [20–23]. Numerous investigations have demonstrated that the incorporation of rare-earth oxides into borate matrices significantly influences phase formation, crystal structure, and physical properties [20, 21].

An understanding of phase equilibria and the physicochemical properties of intermediate phases is a key prerequisite for the targeted synthesis and optimization of novel multicomponent functional materials [24-28].

This work aims to obtain new crystalline and glassy materials in the $Bi_2O_3 – Nd_2O_3·B_2O_3$ system, as well as to study their boundaries of the glass formation region and physical properties.

The $Bi_2O_3–B_2O_3$ system is among the most complex binary oxide systems due to the high tendency of its components to form intermediate compounds of varying composition and structure. Interest in this system stems from the presence of a number of bismuth borates, which possess valuable optical, ferroelectric, and nonlinear optical properties. Furthermore, the compounds in this system are characterized by relatively low melting points, making them promising candidates for the production of glasses, glass-ceramics, and functional crystalline materials.

Phase formation in the $Bi_2O_3–B_2O_3$ system is characterized by the formation of a series of intermediate compounds stable over a wide range of temperatures and compositions. According to the literature [16, 29-31], the system contains five compounds: $Bi_{24}B_2O_{39}$, $Bi_4B_2O_9$, $Bi_6B_{10}O_{24}$, BiB_3O_6, and $Bi_2B_8O_{15}$. The compound $Bi_{24}B_2O_{39}$, which is the richest in bismuth oxide, has a sillenite-type structure and melts incongruently at 632°C. The remaining compounds melt congruently at 675, 722, 708, and 715°C, respectively.

In the range of compositions containing 60–80 mol% Bi_2O_3, the $Bi_{24}B_2O_{39}$ and $Bi_4B_2O_9$ phases form, characterized by high permittivity and promising potential for low-temperature co-sintered ceramics. With increasing boron oxide content, the compounds $Bi_6B_{10}O_{24}$, BiB_3O_6, and $Bi_2B_8O_{15}$ form. Of these, BiB_3O_6 (BiBO) is of greatest practical interest, possessing high nonlinear optical coefficients, a wide transparency range, and high radiation resistance.

Thermodynamic analysis of the system revealed the presence of a melt stratification region in the boron-containing portion of the phase diagram, as well as several eutectic and peritectic transformations that determine the crystallization sequence of the phases. According to modern data [8], the phase relationships in the system are well described by a model comprising five stable and two metastable phases ($BiBO_3$ and $Bi_5B_3O_{12}$). At B_2O_3 contents above ~55 mol.%, a pronounced tendency for the melts to form glass is observed.

According to phase analysis and high-temperature studies, several intermediate phases form in the $Nd_2O_3–B_2O_3$ system. The most reliably identified phases are neodymium orthoborate $NdBO_3$, metaborate $Nd(BO_2)_3$, triborate NdB_3O_6, and tetradecaborate $Nd_4B_{14}O_{27}$ [20, 33-37] The formation of these compounds is determined by the Nd_2O_3/B_2O_3 ratio and the synthesis temperature. In the region rich in neodymium oxide, the stable phase is orthoborate $NdBO_3$, containing isolated triangular $[BO_3]^{3-}$ groups. This compound exhibits high chemical stability and is the most common phase in rare earth borate systems.

With increasing B_2O_3 content, the borate structure progressively becomes more complex due to the formation of chain and network boron-oxygen anions. In the boron-enriched region of the system, metaborate and polyborate phases are formed, characterized by the presence of $[B_3O_6]^{3-}$, $[B_4O_9]^{6-}$, and more complex boron-oxygen fragments. High boron oxide content also promotes the formation of glassy materials containing neodymium as a structure-modifying cation.

Studies of the crystal structure of neodymium borates have shown that the coordination number Nd^{3+} varies over a wide range, which determines the structural diversity of the compounds and their different physical properties [37]

Previously, we studied phase equilibria, glass transition regions, and physical properties of alloys along the sections $Bi_2O_3·B_2O_3–Nd_2O_3$; $Bi_2O_3·B_2O_3–Nd_2O_3·B_2O_3$; $Bi_2O_3·3B_2O_3–Nd_2O_3·B_2O_3$; $3Bi_2O_3·5B_2O_3–Nd_2O_3·3B_2O_3$ [38, 39].

Experimental part

Materials and Synthesis

To study phase equilibria in the Bi_2O_3–Nd_2O_3 B_2O_3 system, alloys of various compositions were synthesized from high-purity oxides. The starting components were bismuth oxide Bi_2O_3 (at least 99.99%), neodymium oxide Nd_2O_3 (at least 99.99%), and boric acid H_3BO_3 (analytical grade). Before weighing, the neodymium oxide was pre-calcined at 1173 K for 10 hours to remove adsorbed moisture and carbonate impurities. Boric acid was used as a precursor to boron oxide; upon heating, it completely dehydrates to form B_2O_3.

The starting material weights were calculated based on the specified composition and weighed on an analytical balance with an accuracy of ±0.0001 g. The resulting mixtures were thoroughly homogenized by grinding in an agate mortar for 30–40 minutes. The powders were then pressed into tablets 8–10 mm in diameter under a pressure of 100–150 MPa.

The samples were synthesized using a solid-phase reaction. To prevent B_2O_3 loss at high temperatures, the samples were placed in tightly sealed corundum crucibles. Heat treatment was performed in stages. In the first stage, the mixtures were heated to 773–823 K at a rate of 50–100 K/h and held for 10–12 hours to remove water and completely decompose the H_3BO_3. After cooling, the products were re-milled, pressed, and further annealed at 973–1173 K for 20–40 hours to complete solid-phase interaction.

To obtain equilibrium samples, the alloys were subjected to multiple cycles of milling, pressing, and annealing. Final heat treatment was performed at temperatures corresponding to the region of existence of the studied phases for 200–300 hours. After annealing, the samples were either air-quenched or furnace-cooled, depending on the experimental objectives.

The resulting alloys were analyzed using X-ray diffraction analysis. The single-phase nature of the samples was determined by the absence of extraneous reflections in the diffraction patterns. Differential thermal analysis and differential scanning calorimetry were additionally used to refine the phase transformation temperatures.

The chosen synthesis technique ensured the achievement of phase equilibrium and the production of samples suitable for constructing an isothermal section of the Bi_2O_3–$Nd_2O_3 \cdot B_2O_3$ system in the subsolidus region.

Methods

Thermal properties and phase transformations in Bi_2O_3–Nd_2O_3 B_2O_3 alloys were studied using differential thermal analysis (DTA). The studies were conducted on a NETZCHSTA 449F3STA – 0836 derivatograph in air. Calcined alumina α-Al_2O_3 was used as the reference material.

Pre-synthesized and homogenized samples weighing 0.3–0.5 g were used for the analysis. The crushed samples were placed in corundum crucibles. Heating was performed from room temperature to 1273–1373 K at a rate of 10 K min^{-1}. After reaching the maximum temperature, the samples were cooled along with the furnace or subjected to repeated heating and cooling cycles to verify the reproducibility of the thermal effects.

Phase transformation temperatures were determined from the positions of endothermic and exothermic peaks on the DTA curves. The onset temperature of the thermal effect was taken as the intersection of the tangent drawn to the steepest portion of the peak with the continuation of the baseline. The temperature determination error was ±5 K.

The thermograms of the studied samples showed effects corresponding to polymorphic transformations, eutectic reactions, melting of intermediate phases, and liquidus processes. For single-phase samples, one or more endothermic effects associated with solid-phase transformations and melting were typically recorded. For two- and three-phase alloys, additional eutectic and peritectic effects were recorded.

The obtained DTA data were used in conjunction with X-ray diffraction analysis results to identify phase transformations, determine melting points, and establish phase equilibria in the studied system. Comparison of thermal effects with the phase composition of annealed samples allowed us to clarify the position of phase regions and the nature of component interactions in the subsolidus and near-liquidus regions of the Bi_2O_3–Nd_2O_3 B_2O_3 phase diagram.

To increase the reliability of the results, each sample was analyzed at least twice. The discrepancy between the thermal effect temperatures obtained in repeated experiments did not exceed 3–5 K, indicating good reproducibility of the measurements.

Physical properties: thermal resistance, electrical resistivity were measured by the compensation method on B7-30 and B7-21A digital voltmeters. The electrical properties of the test samples were studied by measuring their electrical resistance as a function of temperature. Tablet-shaped samples with a diameter of 8–12 mm and a thickness of 1–3 mm were used for the measurements. Silver or platinum electrodes were applied to opposite surfaces of the samples and then thermally annealed to ensure reliable electrical contact.

.

Electrical resistance measurements were performed using a two-probe method with a digital resistance meter in the temperature range of 300–800 K. Temperature was monitored using a thermocouple placed in proximity to the sample. After reaching the set temperature, the sample was held until thermal equilibrium was established, after which the resistance value was recorded.

Result and discussion

Initially, the boundaries of the glass formation region were studied in the ternary system Bi_2O_3–B_2O_3–Nd_2O_3. It is known that only one (Bi_2O_3 - B_2O_3 system) of the binary systems limiting this ternary system has a limited glass transition region.

During our studies, a significant number of glassy alloys were detected in the ternary system. A study of the glass formation region in the system revealed that, despite the absence of glass formation areas in the Bi_2O_3–Nd_2O_3 and B_2O_3–Nd_2O_3 binary systems, the glass formation region in the Bi_2O_3–B_2O_3–Nd_2O_3 ternary system covers a fairly wide area. As can be seen from Figure 1, the glass formation region extends to the boundaries of the B_2O_3–Nd_2O_3 binary system.

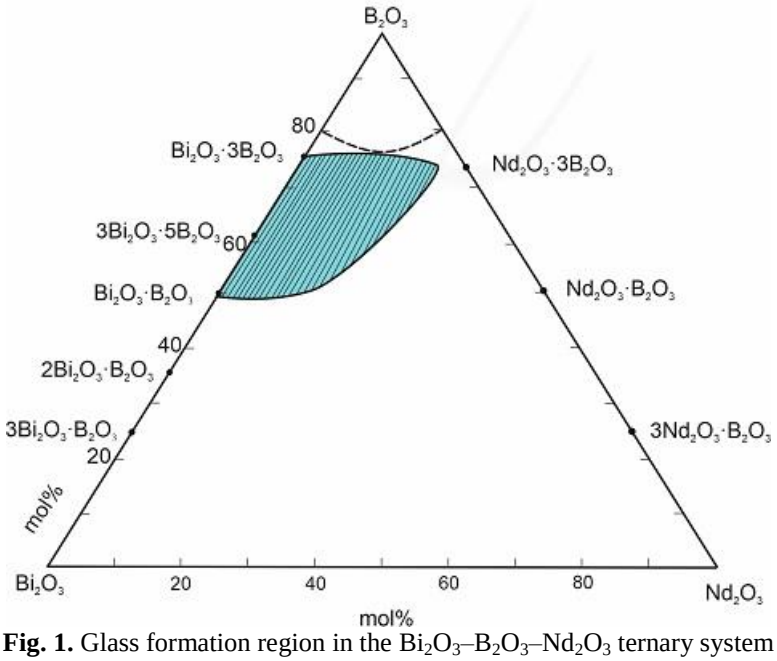


Fig. 1. Glass formation region in the Bi_2O_3–B_2O_3–Nd_2O_3 ternary system

It was found that a new compound consisting of bismuth and neodymium borates was formed in the system. The new compound corresponds to the composition S= $3Bi_2O_3 \cdot Nd_2O_3 \cdot 6B_2O_3$. The obtained compound is glassy purple in color, the crystallization temperature T_c=943K, and the melting temperature T_m=1113K were determined. We believe that the expansion of the glass formation region in this ternary system is due to the presence of this glass-forming compound (S) in the system [38].

The properties of samples №1, containing 95 mol. % Bi_2O_3 – 5 mol. % $Nd_2O_3 \cdot B_2O_3$, №2 85 mol. % Bi_2O_3 – 15 mol. % $Nd_2O_3 \cdot B_2O_3$, №3 75 mol. % Bi_2O_3 – 25 mol. % $Nd_2O_3 \cdot B_2O_3$ from the of the $(Bi_2O_3)_{100-x}$ – $(Nd_2O_3 \cdot B_2O_3)_x$ system, were studied. Based on the obtained results, dependency graphs were constructed and analyzed.

Figure 2 shows the temperature dependences of the thermal conductivity coefficient (curve 1) and thermal resistance (curve 2) of sample №1, containing 95 mol. % Bi_2O_3 – 5 mol. % $Nd_2O_3 \cdot B_2O_3$.

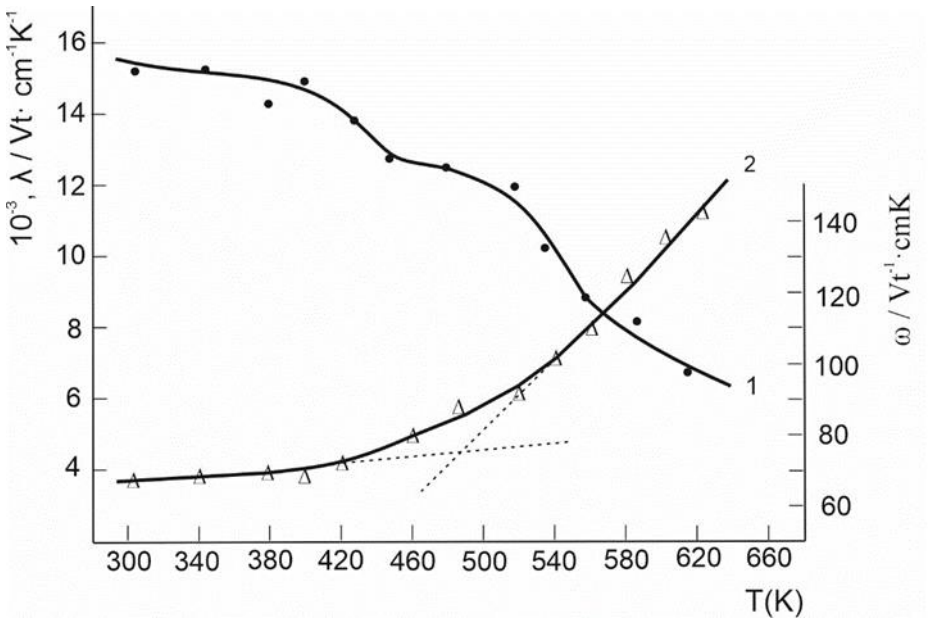


Fig. 2. Temperature dependence of 1- thermal conductivity; 2- thermal resistance of the alloy with composition 95 mol. % Bi_2O_3 – 5 mol. %$Nd_2O_3 \cdot B_2O_3$

The measurements were carried out in the temperature range T=300÷650 K. As can be seen from the graph (curve 1), the overall value of the thermal conductivity coefficient λ(T) decreases with increasing temperature. In the temperature range T=300÷400 K, the value of the thermal conductivity coefficient λ(T) ≈ const, and with a further increase in temperature, a relatively weak decrease in thermal conductivity is observed at T=400÷520 K, and a relatively intense one at T>520 K. For a more accurate study of the λ(T) dependence, the temperature dependence of the lattice thermal resistance ($\omega = 1/\lambda_{lattice}$), which is the inverse value of the lattice thermal conductivity, was analyzed.

Since the electrical conductivity of these compounds is very low ($\sigma \sim 10^{-9} Ohm^{-1}cm^{-1}$), the electron thermal conductivity can be neglected and the total thermal conductivity (λ_{total}) can be approximately taken equal to the lattice thermal conductivity $\lambda_{total} = \lambda_{lattice}$. In other words, the temperature dependence of thermal resistance was established using the formulas $\lambda_{total} = \lambda_{lattice}$ and $\omega = 1/\lambda_{lattice}$. The result obtained is shown in the Figure 2 (curve 2). As can be seen from the graph, the thermal resistance of sample №1 changes nonlinearly

depending on temperature and increases very slightly linearly with increasing temperature in the T=300÷420 K temperature range. In the T ≥ 420 K temperature range, a sharp increase is observed, and the linear increase changes according to a different law. From this, the following general conclusion can be drawn: at relatively low temperatures (T ≤ 420 K), phonons are scattered by point defects and acoustic phonons. As temperature increases, scattering by optical phonons intensifies, and phonon scattering by optical phonons increases. As a result, thermal resistance increases sharply. Therefore, the thermal conductivity and, consequently, the electrical conductivity of this composition are very low

.

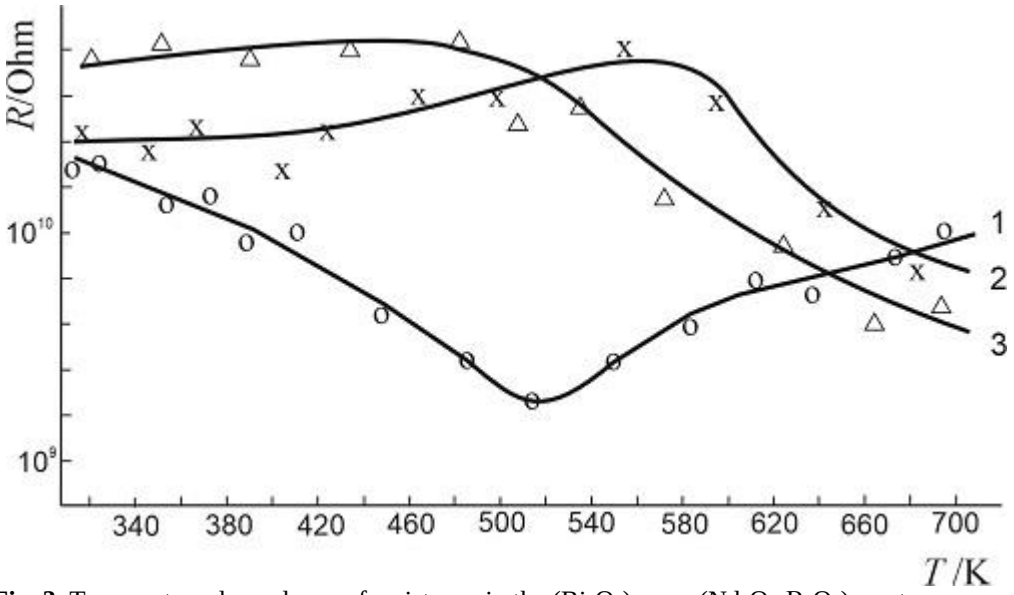


Fig. 3. Temperature dependence of resistance in the $(Bi_2O_3)_{100-x} – (Nd_2O_3 \cdot B_2O_3)_x$ system.
№1-95 mol. % Bi_2O_3 – 5 mol. % $Nd_2O_3 \cdot B_2O_3$
№2-85 mol. % Bi_2O_3 – 15 mol. % $Nd_2O_3 \cdot B_2O_3$
№3-75 mol. % Bi_2O_3 – 25 mol. % $Nd_2O_3 \cdot B_2O_3$

Figure 3 shows the temperature dependences of the electrical resistance (R) of samples №1-3 of the $(Bi_2O_3)_{100-x} – (Nd_2O_3 \cdot B_2O_3)_x$ system. As can be seen from the graphs, with an increase in the $Nd_2O_3 \cdot B_2O_3$ component in the alloys, the value of electrical resistance at a given temperature increases proportionally. On the other hand, different changes are observed in the R(T) dependence of the compositions. Thus, in sample №1, the R value increases after a minimum at a temperature of T = 520 K, ($R_{520} \approx 2.5 \cdot 10^9$ Ohm). In the temperature range T = 300 ÷ 560 K, a monotonic decrease in electrical resistance is observed. At a temperature T> 520 K, a monotonic increase occurs, and at T = 680 K, the electrical resistance $R \approx 1 \cdot 10^{10}$ Ohm.

In sample №2, on the contrary, a partial increase is observed in the temperature range T = 300–560 K and a decrease passing through an extreme point at T = 540 K. The R(T) dependence of this composition resembles the R(T) dependence observed in amorphous materials.

In sample №3, unlike other compositions, the electrical resistance in the temperature range T = 300–480 K is partially constant and decreases with further temperature increase according to the law characteristic of semiconductor materials (R~T~1.0). These observed patterns indicate that the compositions differ in phase structure. Further research is needed to determine the densities of the compositions, the phase structure, and the bonds between the components, as well as the

presence of defects and vacancy centers. At the same time, the change in the R(T) dependence indicates the predominance of the insulator-semiconductor phase. Therefore, the current-voltage characteristics of these compositions were additionally studied.

.

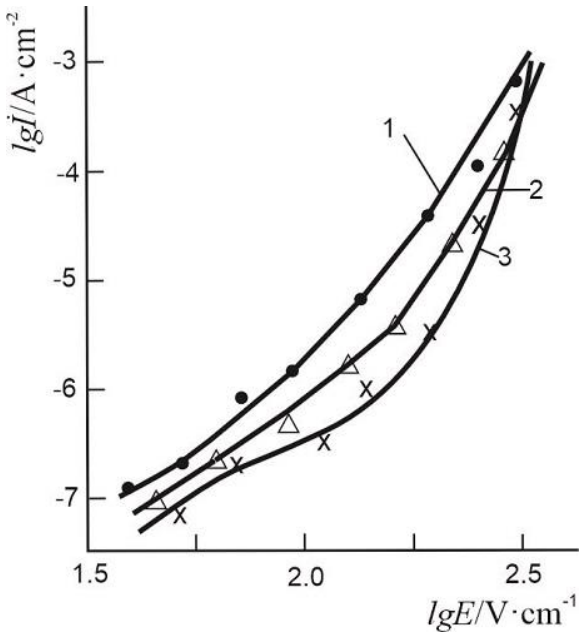


Fig. 4. Volt-ampere characteristics of the compounds in the $(Bi_2O_3)_{100-x} – (Nd_2O_3 \cdot B_2O_3)_x$ system.
1. №1-95 mol. % Bi_2O_3 – 5 mol. % $Nd_2O_3 \cdot B_2O_3$
2. №2-85 mol. % Bi_2O_3 – 15 mol. % $Nd_2O_3 \cdot B_2O_3$
3. №3-75 mol. % Bi_2O_3 – 25 mol. % $Nd_2O_3 \cdot B_2O_3$

Figure 4 shows the current-voltage characteristics of the above alloys of the system. The experimental voltage varied in the range U = 0 ÷ 280 V. As can be seen from the graphs, the current-voltage characteristics of the samples vary non-linearly. In practical terms, the current-voltage characteristic of the sample with composition № 3 is of particular interest. It is known from the literature [40, 41] that the current-voltage characteristics of varistor-type thermistors made of semiconductor materials also vary non-linearly, and their electrical resistances are in the range R ≈ $10^6 \div 10^8$ Ohm. The difference between the compositions we studied and the varistor-type converters cited in the literature is that a higher voltage is required here. The advantage is the possibility of use in a wider temperature range (T = 300 ÷ 440 K).

Figure 5 shows the compositional dependence of the electrical resistance of alloys № 1-3 of the $(Bi_2O_3)_{100-x} – (Nd_2O_3 \cdot B_2O_3)_x$ system. As can be seen from the values of R(T) dependences at temperatures T=300 K and 460 K, the resistance of sample №3 at temperature T=300 K is $R_3=7.8 \cdot 10^{10}$ Ohm, and in the sample with x=5 mol. % $R_1 =2.5 \cdot 10^{10}$ Ohm. That is $R_3/R_1 \approx 3.12$ times more. This shows that with the increase in the concentration of the B_2O_3 component in the compounds, their electrical resistance increases. At temperature T=460K, this difference increases sharply. As can be seen from the graph, the $R_1 \approx 6 \cdot 10^9$Ohm; $R_2 \approx 4 \cdot 10^{10}$ and $(R_3)_{25mol\%} \approx 8 \cdot 10^{10}$Ohm; $R_2/R_1 \approx 4 \cdot 10^{10}/6 \cdot 10^9 \approx 6.67$; $R_3/R_1 \approx 8 \cdot 10^{10}/6 \cdot 10^9 \approx 13.3$ times more, which allows us to say that the increase in temperature is related to the increase in intensity of the component B_2O_3

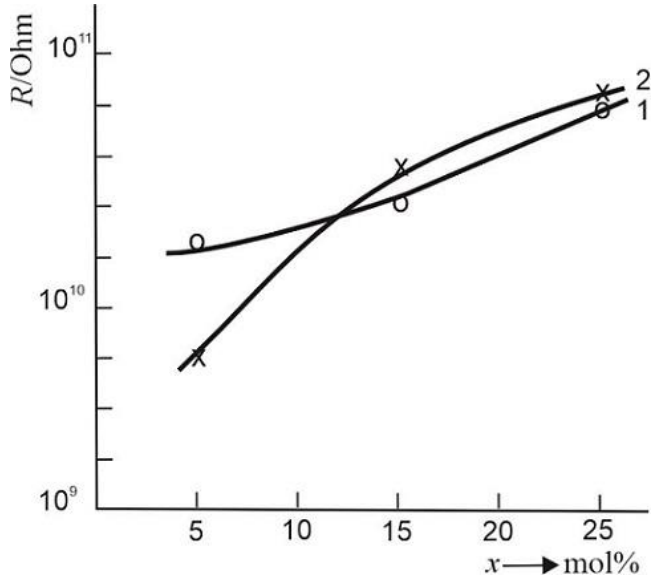


Fig. 5. Composition dependence of electrical resistivity in the $(Bi_2O_3)_{100-x} – (Nd_2O_3 \cdot B_2O_3)_x$ system.

Conclusion

As a result of the conducted studies, it was established that the expansion of the glass transition region in the ternary system Bi_2O_3–B_2O_3–Nd_2O_3 is due to the presence of a glass-forming compound in the system consisting of $3Bi_2O_3 \cdot Nd_2O_3 \cdot 6B_2O_3$.

The nonlinear change in electrical conductivity in the studied alloys of the Bi_2O_3 - $Nd_2O_3 \cdot B_2O_3$ section indicates that the conduction mechanism is due to the hopping displacement of charge carriers. In the $(Bi_2O_3)_{95} – (Nd_2O_3 \cdot B_2O_3)_5$ sample, phonon scattering by point defects and acoustic phonons occurs at relatively low temperatures ($T \leq 420$ K). As the temperature increases, scattering by optical phonons and phonon scattering by optical phonons intensifies. As a result, thermal resistance increases sharply, so the thermal conductivity and, consequently, the electrical conductivity of this alloy become very low. The $(Bi_2O_3)_{75} – (Nd_2O_3 \cdot B_2O_3)_{25}$ alloy can be used to create varistor-type thermistors, applicable in the temperature range of 300–440 K.

References

1. Madiraju S.V.H., Pamula A.S.P. A Brief Guide to the 50 Eco-Friendly Materials Transforming Sustainable Construction. *Austin Environ. Sci.* 2024. V.9. P.1-12. doi.org/10.26420/austinenvironsci.2024.1105
2. Popescu C., Dissanayake H., Mansi E. and Stancu A. Eco Breakthroughs: Sustainable Materials Transforming the Future of Our Planet. *Sustainability*. 2024. V.16. №23. P. 10790. doi.org/10.3390/su162310790
3. Firoozi A. A., Firoozi A. A., Oyejobi D.O., Avudaiappan S., Flores E.S. Emerging trends in sustainable building materials: Technological innovations, enhanced performance, and future directions. *Res. Eng.* 2024. V. 24. P. 103521. doi.org/10.1016/j.rineng.2024.103521
4. Alghamdi A.M. Optical, thermal, mechanical, and antibacterial properties of polyvinyl alcohol/sodium alginate/$ZnMn_2O_4$ nanocomposites films for various optical devices and food packaging applications. *Int.J.Biol.Macromol*. 2024. V.271. P.132689. doi.org/10.1016/j.ijbiomac.2024.132689
5. Zhang Y. and Wang Y. Nonlinear optical properties of metal nanoparticles: a review. *RSC Adv.* 2017. V. 7. № 71. P. 45129-45144. doi.org/10.1039/C7RA07551K
6. Egorysheva A.V., Kargin Yu.F.

7. Phase equilibria in the Bi_2O_3–Al_2O_3–B_2O_3 system. *Russ. J. Inorg. Chem.* 2004. V.49. P. 470–474.
8. Kargin Yu.F., Egorysheva A.V. Phase relations in the solidus region of the Na_2O–Bi_2O_3–B_2O_3 system. *Russ. J. Inorg. Chem*. 2005. V.50. № 12. P.1942–1945.
9. Zeng S., Gong W., Chen Y., Chen Y. Phase diagram and thermodynamics study on the Bi_2O_3–B_2O_3 system for controllable synthesis of the bismuth borate compounds. *Ceram. Int.* 2025. V.51. P. 25416–25425. DOI:10.1016/j.ceramint.2025.03.225
10. P. Becker, Fröhlich R. Crystal Growth and Crystal Structure of the Metastable Bismuth Orthoborate $BiBO_3$. *Z. Naturforsch. B.* 2004. V.59. № 3. P.256-258. DOI:10.1515/znb-2004-0302
11. Bananyarli S.I., Ismayilov Sh.S., Gasimova R.N., Khalilova L.A. Thermophysıcal properties of alloy compositions $(2Bi_2O_3{\cdot}B_2O_3)_{100-x}(2Bi_2O_3{\cdot}3GeO_2)_x$ (x=0, 10, 50). *Azerb. Chem. J.* 2021. №3. P. 44-48. doi.org/10.32737/0005-2531-2021-3-44-48
12. Sammes N.M., Tompsett G.A., Näfe H., Aldinger F. Bismuth based oxide electrolytes—structure and ionic conductivity. *J. Eur. Ceram. Soc.* 1999. V.30. P.1801–1826 DOI:10.1002/chin.199936284.
13. Becker P. Thermal and optical properties of glasses of the system Bi_2O_3 – B_2O_3. *Cryst. Res. and Technol.* 2003. V. 38. P. 74-82. doi.org/10.1002/crat.200310009
14. Hellwig H., Liebertz J., Bohaty L. Linear optical properties of the monoclinic bismuth borate. *J. Appl Phys*. 2000. V. 88. №1. P. 240-244. doi:10.1063/1.373647
15. Kuzmicheva G.M., Melnikova T.I. Structural features of bismuth borates in the system nBi_2O_3-mB_2O_3.*Russ.J.Inorg.Chem*.2009.V.54.№1. P.73-80. DOI:10.1134/S0036023609010148
16. Shaalan M., El-Damrawi G., Hassan A., et al. Structural role of Nd_2O_3 as a dopant material in modified borate glasses and glass ceramics. *J. Mater. Sci: Mater. Electron.* 2021. V. 32. P. 12348-12357. DOI:10.21203/rs.3.rs-194312/v1
17. Bananyarli S.I., Gasimova R.N., Ismayilov Sh.S., Khalilova L.A. Physical and Chemical Research into $(2Bi_2O_3{\cdot}B_2O_3)_{100-x}$–$(2Bi_2O_3{\cdot}3GeO_2)_x$ System and Electrophysical Properties of Obtained Alloys. *Chem. Probl.* 2019. 17(3). P.429–434.
18. Hamidova Sh.F., Kuli-zade E.S., Novruzova F.A., Mehdiyeva S.A. Glass formation in the systems Bi_2O_3-B_2O_3-Ln_2O_3 (Ln - La, Nd, Sm, Yb, Y). *Chem. Probl*. 2015. V.13. P. 209-212. https://chemprob.org/article/glass-formation-in-the-systems-bi2o3-b2o3-ln2o3-ln-la-nd-sm-yb-y/
19. Kothandan D., Kumar R.J. Optical properties of rare earth doped borate glasses. *Int. J. Chemtech Res.* 2015. V. 8. P.310-314
20. Thiel C.W., Thomas Böttger, Cone R.L. Rare-earth-doped materials for applications in quantum information storage and signal processing. *J. Lumin*. 2011. V.131. P.353-361. DOI:10.1016/j. jlumin.2010.12.015
21. Ji Y., Liang J., Chen Z., Xie S. Phase Relations in the System Al_2O_3–B_2O_3–Nd_2O_3, *J. Am. Ceram. Soc.* 1991.V.74. P.444–446. doi.org/10.1111/j.1151-2916.1991tb06906.x
22. Wei X.T., Jiang G.C., Deng K.M., Chen Y.H., Duan C.K., Yin M. Rare-earth doped optical spectral conversion materials with their applications. *Sci. Sin.: Phys. Mech. Astron*. 2012. V. 42. №11. P. 1112 - 1123. https://doi.org/10.1360/132012-783
23. Song J., Kong X., Li C., Jiao J., She Y., Ye N., Hu Z., Wu Y.A. Rare-Earth-Based Borate Optical Crystal with Enlarged Dihedral Angles of Distinct $[BO_3]$ Groups Exhibiting a Wide UV Transparent Range. *Inorg. Chem.* 2024. V.63. №31. P.14786–14793. doi.org/10.1021/acs.inorgchem.4c02759

24. El-shabaan M.M., Mohamed A., Youssif M.I. *et al.* Comparative study on the influence of rare earth ion doping on the structural and optical properties of simple B_2O_3–Na_2O glasses. *Sci Rep*. 2026. V.15. P.35022. https://doi.org/10.1038/s41598-025-21224-x
25. Imamaliyeva S.Z., Huseynova I.F., Daraselia D., et.al. Phase Relations in the Tl_2Te-$TlBiTe_2$-$TlGdTe_2$ Compositions Region of the Tl-Bi-Gd-Te System and Magnetic Properties of the $TlBi_{1-x}Gd_xTe_2$ Solid Solutions. *J. Phase Equilib. Diffus*. 2024. V.45. P.459-468. DOI:10.1007/s11669-024-01096-w
26. Mekhdiyeva I.F., Babayeva, P.H., Aliyev O.A. et al. Phase Equilibria In The Tl_2Te-Tl_5Te_3-Tl_9ErTe_6 system. *New Mater. Compd. Appl*. 2019. V.3. №3. P.142-149.
27. Huseynova I.F., Bayramova N.A., Imamaliyeva S.Z. et al. Phase Equilibria in the Ag_8GeSe_6–Ag_7GeSe_5I–$GeSe_2$ System. *Russ. J. Inorg. Chem*. 2025. V.70. №11. P.1794–1803. doi.org/10.1134/S0036023625602533
28. Gurbanov N.A., Imamalizade Ch.A., Gardashova L.A. et al. Investigation of the composition– phase-transformation temperature relationship in the NiTi-based alloys using machine learning. *Prog. Phys. Met.* 2026. V.27 (2). P. 278 – 303. DOI:10.15407/ufm.27.02.278
29. Imamalizade Ch.A., Manufacturing of nitinol-based alloys by using modern technology: A short review // Physics and Chemistry of Solid State, 202023, V.24(2). P. 341 - 347
30. Levin E.M., McDaniel C.L. The System Bi_2O_3–B_2O_3. *J. Am. Ceram. Soc*. 1962. V.45. №8. P.355–360. DOI:10.1111/j.1151-2916.1962.tb11168.x
31. Kargin Y.F., Zhereb V.P., Egorysheva A.V. Phase diagram for metastable states of Bi_2O_3-B_2O_3 system. *Russ. J. Inorg. Chem*. 2002. V.47. № 8. P.1362-1364.
32. Boonin K., Kaewkhao J., Ratana T., Limsuwan P. Preparation and Properties of Bi_2O_3-B_2O_3-Nd_2O_3 Glass System. Procedia Eng. 2011. V.8. P.207-211. DOI:10.1016/j.proeng.2011.03.038
33. Varsamis C.P.E., Makris N., Valvic C., Kamitsos E.I. Short-range structure, the role of bismuth and property–structure correlations in bismuth borate glasses. *Phys. Chem. Chem. Phys*.2021. V.23. № 16. P. 10006-10020. DOI: 10.1039/d1cp00301a
34. Jakobsson L.K., Tranell G., Jung I.H. Experimental Investigation and Thermodynamic Modeling of the B_2O_3-FeO-Fe_2O_3-Nd_2O_3 System for Recycling of NdFeB Magnet Scrap. *Metall. Mater. Trans. B.* 2017. V. 48. P. 60-72. DOI: 10.1007/s11663-016-0748-0
35. Ji Y., Liang J., Chen Z., Xie S. Phase relations in the system BaO–Nd_2O_3–B_2O_3 ($B_2O_3 \geq 50$ mol%) and crystal growth of $NdBaB_9O_{16}$. *J. Cryst. Growth*. 1994. V.137. №3. P.521–527. DOI: 10.1016/0022-0248(94)90993-8
36. Kuznetsov A.B., Jamous A.Y., Svetlichnyi V.A., Kokh K.A. Phase relations between $Na_3Nd(BO_3)_2$, $Na_3Nd_2(BO_3)_3$ and $NdBO_3$ and their luminescence properties. *J. Struct. Chem.* 2024. V. 65. №9. P.131995. DOI:10.26902/JSC_id131995
37. Kuzmin N., Maltsev V., Mikliaeva E., Volkova E., Boldyrev K., Koporulina E. Phase Relations in the Ln_2O_3–Cr_2O_3–B_2O_3 (Ln=Gd–Lu) Ternary Oxide Systems. *Materials*. 2023. V.16. №5. P. 1831. doi.org/10.3390/ma16051831
38. Müller-Bunz H., Nikelski T., Schleid T. Single crystals of the neodymium (III) meta-borate $Nd(BO_2)_3$ and ortho-borate $Nd[BO_3]$. *Cheminform*. 2003. V.58. P.375–380. DOI:10.1002/chin.200334004
39. Bananyarli S.I., Ismayilov Sh.S., Gasimova R.N., Khalilova L.A. Study of $3Bi_2O_3 \cdot 5B_2O_3$-$Nd_2O_3 \cdot 3B_2O_3$ system and dependence of electrophysical and heat properties of obtained alloys on the composition. *Chem. Probl.* 2020. V. 18. P.

106-112. DOI:10.32737/2221-8688-2020-1-106-112
40. Bananyarli S.I., Ismayilov Sh.S., Khalilova L.A. Study of heat and electrophysıcal propertıes of system alloys $Bi_2O_3 \cdot B_2O_3$-Nd_2O_3. *DSJ*. 2022. V.64. P.11-15. DOI:10.32737/2221-8688-2020-1-106-112
41. Valeev Kh.S., Kvaskov V.B. *Energoizdat*. 1983. 160 P. (in Russian)
42. Lyashkov A., Tonkoshkur A. Varistor composites with a positive temperature coefficient of resistance. *Tech. Phys*. 2011. V.56. №3. P. 427-428. DOI:10.1134/S1063784211030121

Bi_2O_3 - B_2O_3 - Nd_2O_3 ÜÇLÜ SİSTEMİNDƏ ŞÜŞƏƏMƏLƏGƏLMƏ SAHƏSİNİN SƏRHƏDLƏRİN MÜƏYYƏN EDİLMƏSİ, Bi_2O_3 - $Nd_2O_3 \cdot B_2O_3$ KƏSİYİNDƏ BƏZİ TƏRKİBLƏRİN İSTİLİK VƏ ELEKTROFİZİKİ XASSƏLƏRİN TƏDQİQİ.

S.İ.Bənənyarlı, L.Ə.Xəlilova, Ç.A.İmaməlizadə, Ş.S.İsmayılov

Bu məqalədə Bi_2O_3 - B_2O_3 - Nd_2O_3 üçlü sistemi DTA və RFA metodları ilə öyrənilmiş, şüşəmələgəlmə sahəsinin sərhədləri təyin edilmiş, Bi_2O_3 - $Nd_2O_3 \cdot B_2O_3$ kəsiyindən bəzi tərkiblərin elektrik və istilik xassələri tədqiq edilmişdir. Bi_2O_3–B_2O_3–Nd_2O_3 üçlü sistemində şüşəmələgəlmə sahəsinin genişlənməsi, sistemdə şüşəmələgətirən $3Bi_2O_3 \cdot Nd_2O_3 \cdot 6B_2O_3$ tərkibli birləşmənin olması ilə əlaqədar olduğu təsbit edilmişdir. Müəyyən edilmişdir ki, $(Bi_2O_3)_{95}$ – $(Nd_2O_3 \cdot B_2O_3)_5$ tərkibli nümunədə nisbətən ağağı temperaturlarda ($T \leq 420K$) fononların nöqtəvi defektlərdən və akustik fononlardan səpilməsi baş verir. Temperaturun artması ilə optik fononlardan səpilmə intensivləşir və fononların optik fononlardan səpilməsi güclənir. Nəticədə istilik müqaviməti kəskin artır. Ona görə də bu tərkibin istilikkeçiriciliyi və uyğun olaraq elektrikkeçiriciliyi çox kiçikdir. Təcrübələr nəticəsində müəyyən edilmişdir ki, $(Bi_2O_3)_{75}$ – $(Nd_2O_3 \cdot B_2O_3)_{25}$ tərkibli nümunədə volt-amper xarakteristikası qeyri-xətti dəyişir, elektrik müqaviməti $R \approx 10^6 \div 10^8$ Om tərtibindədir. Bu da qeyd olunan tərkibdən praktikada 300÷440K temperatur intervalında varistor kimi termorizistorların istehsalında istifadə etməyə imkan verir.

Açar sözlər: *istilik müqaviməti, istilikkeçirmə, fonon, yarımkeçirici, termorezistor, varistor.*